energies

MDPI

Article

A Method for CM EMI Suppression on PFC Converter Using Lossless Snubber with Chaotic Spread Spectrum

Weifeng Fan *, Yilong Shi and Yanming Chen

School of Electrical Engineering, Guangxi University, Nanning 530004, China
* Correspondence: fwf2022@163.com

Abstract: This paper proposes an improved common mode (CM) electromagnetic interference (EMI) suppression method in switching power supplies. The lossless snubber circuit can reduce du/dt and EMI in the high-frequency band. Nevertheless, it has a weak EMI suppression effect on the low-frequency band. A method combining the chaotic spread spectrum and the lossless snubber (CSS–LS) is proposed to improve the EMI suppression effect of the lossless snubber. It is an effective means to suppress CM EMI further. The paper used a Boost PFC converter as the object of analysis to study the CM EMI suppression effect of CSS–LS. Firstly, a CM EMI-equivalent model of the lossless snubber PFC converter was established. Then, the power spectral density function under chaotic spread-spectrum modulation was derived. The simulation analysis was performed. Finally, an experimental prototype was built, and relevant EMI tests were carried out. The experimental results show that CSS–LS can reduce CM EMI by 4~20 dBμV with little impact on converter stability. Fewer extra costs are needed for this optimization method, which is suitable for high-power-density power electronic devices.

Keywords: PFC converter; lossless snubber; chaotic spread spectrum; common-mode electromagnetic interference; power spectral density

Citation: Fan, W.; Shi, Y.; Chen, Y. A Method for CM EMI Suppression on PFC Converter Using Lossless Snubber with Chaotic Spread Spectrum. *Energies* **2023**, *16*, 3583. https://doi.org/10.3390/en16083583

Academic Editor: Anna Richelli

Received: 31 March 2023
Revised: 19 April 2023
Accepted: 19 April 2023
Published: 21 April 2023

1. Introduction

In recent years, wide forbidden-band semiconductor devices, such as silicon carbide and gallium nitride, have been widely used. Power electronic converters operate at higher switching frequencies [1,2]. Higher frequencies require power-switching devices to have faster turn-on and turn-off speeds. Faster switching speeds increase the voltage and current change rates of power-switching devices. Excessive voltage and current change rates can cause overvoltage and overcurrent in the device, which will cause damage to the device. Generally, du/dt is used to express the voltage change rate, and di/dt is used to express the current change rate. In addition to damaging the device, du/dt and di/dt also produce noise that interferes with other electrical devices [3–5]. Moreover, at higher switching frequencies, the influence of the converter circuit distribution parameters is more prominent. It poses new challenges to electromagnetic compatibility (EMC) issues [6,7].

High-speed jump voltage and current generate electromagnetic interference (EMI) through near-field coupling and conductive media [8]. This EMI will enter the grid through the input power lines, which will cause conducted EMI problems. Conducted EMI may cause signal distortion, voltage fluctuation, surge voltage, grid pollution, and other problems. Therefore, the conducted EMI can affect the regular operation of the device and other power-using devices on the same grid [9–11]. Especially in microgrids, the effect of conducted EMI is more serious. Therefore, it is essential to study and suppress the conducted EMI [12–14]. Conducted EMI is usually divided into common mode (CM) and differential mode (DM) noise. Compared to DM EMI, CM EMI is more extensive in magnitude and higher in frequency. Furthermore, CM EMI can be radiated through the wire [15]. It is generally believed that CM noise has a more significant impact on the regular operation

of a circuit. So, suppressing CM noise has a more theoretical significance and practical engineering application [16].

Nowadays, using EMI filters is a conventional and effective method of CM EMI suppression. The EMI filter can be divided into passive EMI filter (PEF) and active EMI filter (AEF). PEFs are relatively simple to design and have a wide range of applications [17–20]. However, to effectively suppress CM EMI, the size and weight of PEFs are relatively large. The excessive weight and volume are not conducive to the high-density design of power electronic converters. Compared to PEFs, AEFs are smaller and lighter, which allows for a better integration degree of the converter using the AEF [21–23]. Nevertheless, due to the bandwidth limitation of active devices, AEFs have poor CM EMI suppression in the high-frequency band. In addition, the control signal's spread-spectrum pulse-width modulation is also a CM EMI suppression method. In recent years, chaotic spread-spectrum techniques have received much attention from scholars. Because the chaotic spread spectrum can reduce the noise from the circuit at the source, it is easy to implement. Moreover, it has a better spread-spectrum effect than the periodic spread spectrum. Many papers demonstrate the effect of the chaotic spread spectrum in suppressing EMI [24,25]. Reducing du/dt is another effective method of CM EMI suppression. Larger du/dt through the distributed capacitance will cause CM noise [26].Therefore, reducing du/dt can reduce CM noise. Snubber capacitors and soft switching are usually conventional methods to reduce du/dt [27,28]. However, snubber capacitors can cause excessive turn-on losses. Soft switching requires additional auxiliary circuits in single-phase power factor correction (PFC) circuits. It increases the circuit's cost, and the converter becomes more complex. Lossless snubber circuits have lower switching losses than conventional snubber circuits because the lossless snubber circuit transfers the energy in the snubber capacitor to the load or back to the power supply after the power device is turned off. The energy is not consumed internally. It reduces switching losses and increases the converter's efficiency [29]. Furthermore, a passive lossless snubber circuit uses only a small number of passive components. It does not increase the complexity of the control circuit. Therefore, the lossless snubber has been widely used in PFC circuits.

Most research on snubber circuits focuses on the operating principle and circuit topology. The EMI suppression effect is only shown as an experimental result. The experimental results of [30] show that passive lossless snubber circuits can suppress high-frequency EMI. In [31], a new lossless snubber circuit is proposed for flyback converters. This snubber circuit has a significant effect on radiation interference suppression. However, the EMI suppression effect is poor in the conducted interference band (150 kHz~30 MHz). In [32], the effect of the RC buffer circuit on the switching oscillation is analyzed. This paper indicates that increasing snubber capacitance can reduce the low-frequency oscillation and EMI. However, excessive snubber capacitance will cause high-frequency oscillation. It does not contribute to the stability of the converter. The snubber circuit has the problem of poor EMI suppression in the relatively low-frequency band (typically 150 kHz~5 MHz). For this problem [33] proposes a combination of zero-voltage switching (ZVS) and periodic spread-spectrum modulation EMI suppression method. This method effectively reduces the low-frequency EMI. However, it increases the design difficulty of the control circuit.

In order to improve EMI suppression, this paper proposes an improved method based on the chaotic spread spectrum and the lossless snubber (CSS–LS). CSS–LS improves CM EMI suppression of the lossless snubber. At the same time, CSS–LS has better CM EMI suppression in the high band compared to the conventional chaotic spread spectrum. Moreover, CSS–LS can reduce the converter's switching loss and increase the converter's efficiency. This method does not need to occupy much space. So, it can be integrated into the converter circuit. Furthermore, considering the widespread use of lossless snubber circuits in Boost PFC converters, this paper takes the passive lossless buffer Boost PFC converter as the research object. The Boost PFC converter has a high power factor. Therefore, it is often used in AC–DC applications. Moreover, because the PFC converter is directly connected to the input power supply, its EMI problem is severe. Reducing the EMI of the PFC converter

can prevent the grid from being polluted and other power equipment from being affected. At the same time, because of the simple structure of the Boost PFC converter, the CM EMI conduction path of the lossless absorption PFC converter can be analyzed explicitly.

In the following Section 2, the principles of nondestructive absorption will be presented. The CM EMI conduction path of lossless snubber PFC converters is analyzed. Then, a CM EMI-equivalent model is constructed. The principle of EMI suppression by the snubber circuit is revealed. Moreover, Section 3 explains the principles of CSS–LS. On this basis, the power spectral density function of the drain–source voltage under CSS–LS is derived. In Section 4, the simulation analysis is completed. The simulation results verify the accuracy of the theoretical derivation. In Section 5, the experimental platform is built. Related EMI tests were conducted on the converter. The experimental results show that CSS–LS reduces the CM EMI by 4~20 dB μV and has little effect on the converter stability.

2. Lossless Snubber PFC Converter

2.1. Principle of the Lossless Snubber

Passive lossless snubber circuits can be used in various power electronic converters. Their structure is relatively universal. CM noise dominates the conducted EMI in slight to medium power Boost PFC converters. This paper, therefore, takes a low-power PFC converter as the object of study. The CM EMI suppression effect of a lossless snubber circuit is analyzed, while other disturbances caused by complex topologies can be reduced.

A Boost PFC converter topology with a passive lossless snubber circuit is shown in Figure 1. Inductor L, switching S, diode VD_0, and output capacitor C_o form the main circuit of the PFC converter diodes. VD_1, VD_2, VD_3, inductor L_r, and capacitors C_r and C_s in the dashed box form the passive lossless snubber circuit.

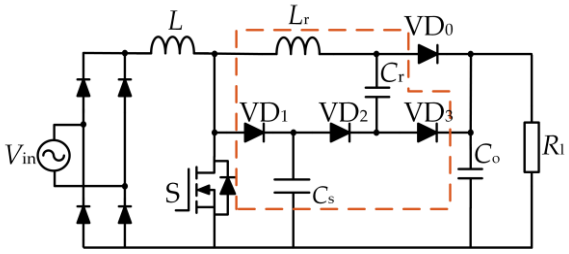

Figure 1. Lossless snubber Boost PFC circuit topology.

The principle of a lossless snubber circuit to reduce the du/dt of the converter is as follows: When the switching is disconnected, the rate of rise of the drain–source voltage (v_{ds}) is limited by C_s. Afterward, the lossless snubber circuit transfers the energy from the snubber circuit to the load by resonance, and its operating modes are shown in Figure 2. In mode 1, the switch is in the off-state, the same as when switched off in a conventional PFC converter. In mode 2, the switch turns on, and the current flowing through L_r decreases linearly. Because the switching frequency is much greater than the operating frequency, the input current i_{in} can be approximated as constant over one switching cycle. Then, the drain–source current i_d starts to rise linearly. L_r has a significant impact on mode 2. A large L_r can reduce the rising rate of i_d. However, too large L_r will make mode 2 last too long and affect the whole process of the lossless snubber circuit. In mode 3, diode VD_0 turns off, and VD_2 turns on after the current flowing through L_r drops to zero. C_s, C_r, and L_r start the first resonance process. The energy on C_s is gradually transferred to C_r and L_r in this mode. Mode 3 ends when the energy transfer in C_s is complete. In mode 4, the voltage across C_s drops to zero. At this time, VD_1 is on. In addition, C_r and L_r carry out the second resonance process through VD_1 and VD_2. The energy on L_r is transferred to C_r. When the energy transfer in L_r is completed, mode 4 ends. In mode 5, the second resonance process ends. This mode coincides with the conventional PFC converter when the switching is on. The energy of the snubber circuit is stored in C_r. In mode 6, the switching is off. However, v_{ds} cannot change rapidly due to the presence of C_s. C_s limits the rising rate of v_{ds}. C_s

plays a significant role in this mode. A suitable value of C_s can effectively reduce du/dt. Nevertheless, too large a C_s can affect the resonance process and reduce the stability of the converter. Meanwhile, in mode 6, VD_3 conducts. The energy in C_r is transferred to the load, which realizes the lossless operation of the lossless snubber circuit.

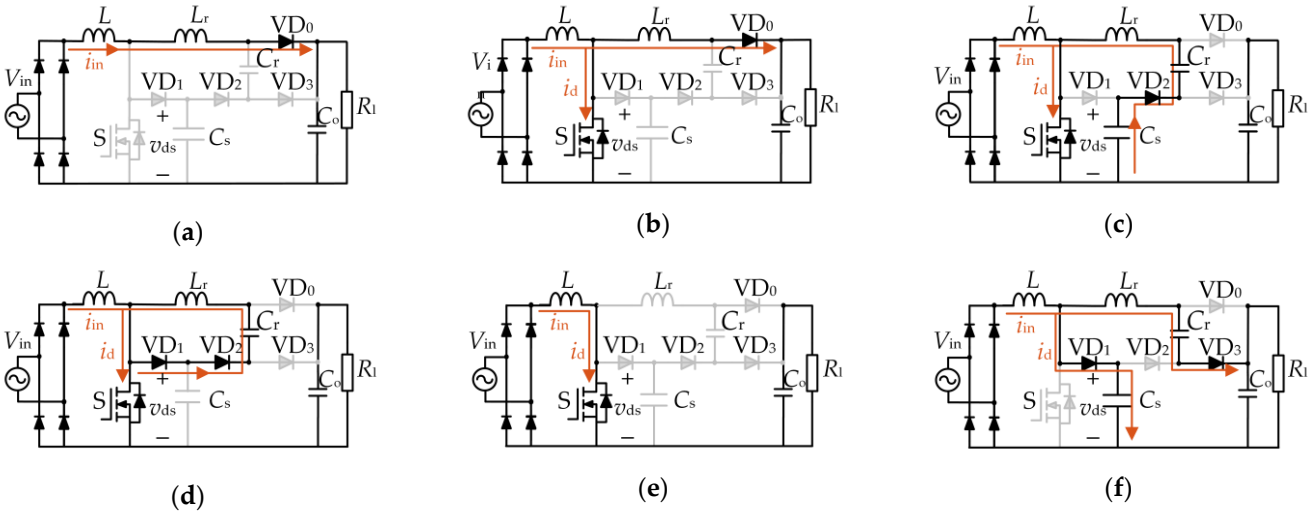

Figure 2. Operating modes of lossless snubber PFC: (**a**) Mode 1; (**b**) Mode 2; (**c**) Mode 3; (**d**) Mode 4; (**e**) Mode 5; and (**f**) Mode 6.

The operating principle of the lossless snubber circuit shows that the snubber circuit mainly relies on the snubber capacitor to suppress the du/dt of the switching tube. Because the lossless snubber circuit can transfer the energy from the snubber circuit to the load through resonance, its opening loss is smaller than that of the conventional snubber circuit. Therefore, without affecting the regular operation of the converter, the lossless snubber circuit can choose a larger capacitance snubber capacitor to obtain a better du/dt suppression effect.

2.2. Equivalent Model of CM EMI

To clarify the impact of du/dt on the CM EMI, the CM EMI conduction path of the lossless snubber PFC converter was first analyzed. When using the linear impedance stabilization network (LISN) for EMI measurements, the CM EMI conduction path is shown in Figure 3.

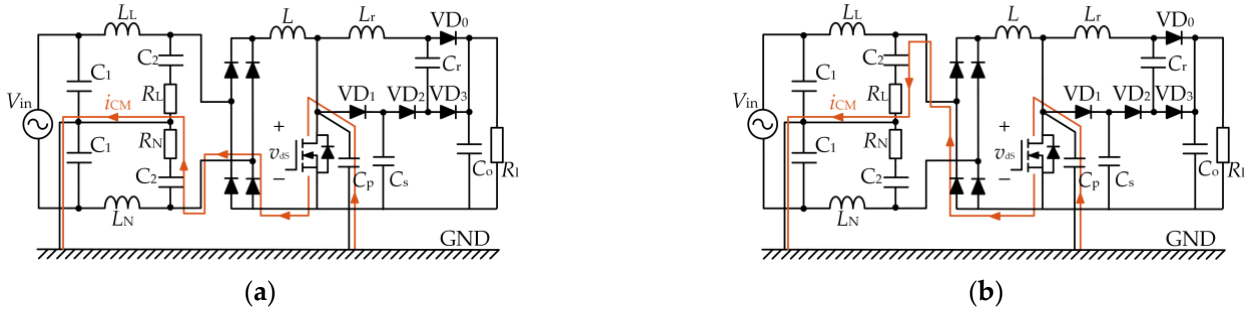

Figure 3. Conduction of CM EMI: (**a**) Positive half-cycle of input voltage and (**b**) Negative half-cycle of input voltage.

According to Figure 3, during switching, the high-speed jump of v_{ds} forms a CM noise conduction loop through the parasitic capacitance C_p between the switch heat sink and the protective ground. Moreover, the CM current i_{CM} causes CM EMI through the noise conduction loop.

In order to quantify and analyze the principle of nondestructive snubber circuits to suppress CM EMI, the CM EMI conduction loop is equated. The voltage across the LISN resistor was used to measure the magnitude of the CM EMI. We denoted the voltage of resistor R_L on the L line as v_L and the voltage of resistor R_N on the N line as v_N. The CM noise voltage v_{CM} can be quantified as:

$$v_{CM} = (v_L + v_N)/2 \quad (1)$$

Because C_p is usually very small, its value is only a few tens of pF, and C_1 = 1 μF and C_2 = 0.1 μF in LISN. Therefore, the CM noise equivalent circuit can be obtained by combining Equation (1) with the conduction path of CM EMI, as shown in Figure 4. In this figure, $R_{LN} = R_L/2 = R_N/2 = 25\ \Omega$. As shown in Figure 4, the high-speed jump v_{ds} is the primary noise source of CM noise. So, suppressing du/dt can directly reduce CM EMI.

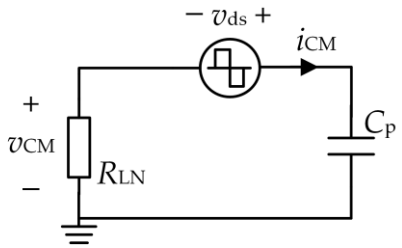

Figure 4. Equivalent circuit of CM EMI.

2.3. CM EMI Suppression Effect of Snubber Circuit

As v_{ds} is the primary source of CM noise, the analysis of the CM EMI suppression effect of the snubber circuit can be equated to the analysis of the effect of the snubber circuit on the v_{ds} spectrum. The v_{ds} waveform is usually approximated as a trapezoidal waveform to simplify the analysis. Decomposing v_{ds} into Fourier steps, the amplitude of each harmonic can be obtained as:

$$A(k) = 2A_t\tau_w f_s \left|\sin c(k\pi f_s \tau_w)\right| \left|\sin c(k\pi f_s \tau_r)\right| \quad (2)$$

In Equation (2), k = 1,2,3, . . . , denotes the number of harmonics. The function $A(k)$ represents the amplitude of the kth harmonic. The function sinc(x) = sin$x$/x. A_t is the amplitude of the trapezoidal wave; f_s is the switching frequency; τ_w is the time between the voltage rising to $A_t/2$ and falling to $A_t/2$, and τ_r is the rise and fall time of the voltage.

Due to the fast switching speed of the power-switching devices, the drain–source voltage's rise and fall times are short. So, there is $\tau_w >> \tau_r$. According to Equation (2), the envelope of the harmonic amplitude decays with a slope of −20 dB/dec when the number of harmonics is greater than $1/(\pi f_s \tau_w)$. When the number of harmonics is greater than $1/(\pi f_s \tau_r)$, the decay slope is −40 dB/dec. Increasing the snubber capacitance suppresses du/dt and reduces the rate of rise of v_{ds}. When the higher harmonics start to decay at a relatively low number of times with a slope of −40 dB/dec, this reduces the CM noise at high frequencies. However, to ensure the converter's regular operation, the value of the snubber capacitor should not be too large, resulting in a lossless snubber circuit for the relatively low-frequency band of the CM noise suppression effect that is poor.

3. Principles of CSS–LS

To improve the low-frequency EMI suppression of the lossless snubber circuit and to further reduce the CM noise of the circuit. The lossless snubber Boost PFC converter was optimized using chaotic spread-spectrum modulation.

Chaos spread spectrum reduces the noise peak at the switching frequency and its multiples by extending the switching spectrum. At the same time, the chaotic spread spectrum has been widely used in various power electronic converters because it does not change the circuit structure or add additional hardware. The key to achieving chaotic

spread-spectrum modulation is to make the switching frequency of the switching converter vary chaotically within a specific range. After using chaotic spread-spectrum modulation, the PWM and the drain–source voltage waveforms of the switching are shown in Figure 5.

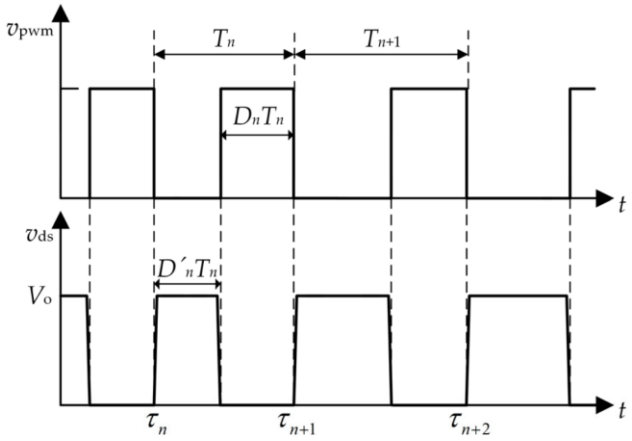

Figure 5. Waveforms of PWM and drain–source voltage.

In Figure 5, V_o is the output voltage amplitude. τ_n is the starting moment of the nth switching cycle. T_n is the duration of the nth switching cycle. D_n is the duty cycle of the nth switching cycle, and $D'_n = 1 - D_n$. The slope of the voltage rise when the switching tube is switched off was approximated as K. The slope of the voltage fall was approximated as $-K$.

According to Figure 5, the time domain equation for v_{ds} is:

$$v_{ds}(t) = \sum_{n=1}^{\infty} v_{dsn}(t - \tau_n) \tag{3}$$

In Equation (3), $v_{dsn}(t)$ is

$$v_{dsn}(t) = \begin{cases} Kt, & 0 < t \leq t_1 \\ V_o, & t_1 < t \leq t_2 \\ V_o - K(t - t_2), & t_2 < t \leq D'_nT_n \\ 0, & \text{Others} \end{cases} \tag{4}$$

where 0 to t_1 is the switching-off process. t_1 to t_2 is the switching-off time. t_2 to D'_nT_n is the switching-on process, and the slope of voltage rise $K = V_o/t_1$.

Because τ_n is the accumulation of the first $n - 1$ switching periods, τ_n is a chaotic sequence. A time-continuous function $N(t)$ is defined from τ_n [34]. $N(t)$ denotes the number of v_{ds} trapezoidal waves in the time interval [0,t].

$$N(t) = \max\{n : \tau_n < t\} \tag{5}$$

For $\tau_{N(T)} \leq T \leq \tau_{N(T)+1}$, the spectrum of $v_{ds}(t)$ is:

$$\begin{aligned} V_{dsT}(jf) &= \sum_{n=1}^{N(t)} V_{dsn}(jf)e^{-j2\pi f\tau_n} \\ &= \sum_{n=1}^{N(t)} V_o(D'_nT_n - t_1)\text{sinc}(\pi f t_1)\sin(D'_nT_n - t_1)e^{-j\pi f(2\tau_n + D'_nT_n)} \end{aligned} \tag{6}$$

In order to analyze the energy distribution of v_{ds} at fundamental and octave frequencies, a replacement representation can be made using the power spectral density. The power spectral density is often used to characterize the distribution of the power of a signal in the frequency domain. The power spectral density $P(f)$ of v_{ds} after chaotic spreading is calculated from $V_{dsT}(jf)$ and can be expressed as:

$$P(f) = \lim_{T\to\infty} \frac{1}{T} E(|V_{dsT}(jf)|^2) \tag{7}$$

where E(·) is the expectation function.

Substituting Equation (6) into Equation (7), and $|V_{dsT}(jf)|^2$ is calculated as:

$$|V_{dsT}(jf)|^2 = \frac{V_o^2}{2\pi^2 f^2}\operatorname{sinc}^2(\pi f t_1) \times \begin{bmatrix} N(t) - \sum_{i=1}^{N(t)} \cos 2\pi f(D\prime_i T_i - t_1) \\ + \sum_{i=1}^{N(t)} \sum_{m=1}^{N(t)-i} \cos 2\pi f\left(\Delta\tau + \frac{\Delta T}{2} + \frac{D\prime_i T_i - D\prime_m T_m}{2}\right) \\ + \sum_{i=1}^{N(t)} \sum_{m=1}^{N(t)-i} \cos 2\pi f\left(\Delta\tau + \frac{\Delta T}{2} - \frac{D\prime_i T_i - D\prime_m T_m}{2}\right) \\ - \sum_{i=1}^{N(t)} \sum_{m=1}^{N(t)-i} \cos 2\pi f\left(\Delta\tau + \frac{\Delta T}{2} + \frac{D\prime_i T_i + D\prime_m T_m}{2} - t_1\right) \\ - \sum_{i=1}^{N(t)} \sum_{m=1}^{N(t)-i} \cos 2\pi f\left(\Delta\tau + \frac{\Delta T}{2} - \frac{D\prime_i T_i + D\prime_m T_m}{2} + t_1\right) \end{bmatrix} \quad (8)$$

where $\Delta\tau = \tau_i - \tau_m$ and $\Delta T = T_i - T_m$. Because τ_n and T_n are chaotic sequences, $\Delta\tau$ and ΔT are chaotic variations.

Due to the wild and ergodic nature of the chaotic sequences, the double summation term in Equation (8) shows that the distribution of the v_{ds} spectrum after spreading is uniform compared to that before spreading. Combining Equation (7) with Equation (8) shows that CSS–LS makes the energy of v_{ds} concentrated at the switching frequency, and its multiples are spread over a frequency band with a specific bandwidth. This results in a reduced and continuous peak in the power spectral density of the v_{ds}.

4. Simulation Analysis

In order to verify the accuracy of the above theoretical derivation, this chapter used the simulation software Saber 2016 to simulate the CM EMI suppression effect of the lossless snubber and CSS–LS. A Boost PFC converter simulation model with a lossless snubber circuit was built, and the simulation parameters are shown in Table 1.

Table 1. Simulation parameters of Boost PFC converter.

Parameters	Value
Input Voltage V_{in}	15~24 V
Output Voltage V_o	48 V
Inductance L	170 μH
Output Capacitance C_o	2200 μF
Load resistance R_l	20 Ω
Switching Frequency f_s	100 kHz

UC3854 was selected for the controller of the PFC converter. The switch was selected as IRFP460. Considering the relationship between C_s and switching losses, the value of C_s can be calculated by the following equation [35]:

$$C_{sopt} = \frac{i_d R_g C_{dg}}{v_g} \quad (9)$$

where C_{sopt} is the optimal value of C_s, R_g is the gate drive resistor, C_{dg} is the gate–drain parasitic capacitance of the switching tube, and v_g is the gate–drive voltage.

After calculations and simulation tests, C_s was taken to be 4.7 nF. The resonant capacitor C_r requires storing the energy of the lossless snubber circuit, and its value is usually 10~30 times that of C_s. The final value of 47 nF was taken for this design.

The analysis of the lossless snubber circuit's operating mode shows that two resonance processes exist in the lossless snubber circuit. In order to ensure that the resonance process does not affect the regular operation of the converter, the resonance should be completed within the time of the switching tube conduction. Therefore, the resonance parameters need to satisfy the following:

$$\begin{cases} \frac{1}{2\pi\sqrt{L_r C_r}} > \frac{f_s}{D_{min}} \\ \frac{1}{2\pi\sqrt{L_r C_{eq}}} > \frac{f_s}{D_{min}} \end{cases} \quad (10)$$

where $D_{min} = (1 - V_{in\_max}/V_o)$ is the minimum duty cycle of the PFC converter, and $C_{eq} = C_r C_s/(C_r + C_s)$.

Without affecting the regular operation of the converter, the larger the value of the L_r, the better the buffering effect of the lossless snubber circuit. So, L_r was chosen as 1 μH in this design.

In order to analyze the effect of the lossless snubber circuit, the primary and lossless snubber PFC converters were simulated. The PFC converter was set up according to the Application note about UC3854 from Texas Instruments. The simulation circuit diagram is shown in Figure 6. The chaotic signal for the spread spectrum was generated by Chua's circuit. Chua's circuit is a third-order nonlinear circuit. It mainly consists of a linear circuit and a nonlinear circuit. Figure 7 shows a typical Chua's circuit. In Figure 7, the elements in the dashed box form a nonlinear negative resistor. With correctly set parameters, the voltages across C_1, C_2, and L vary chaotically.

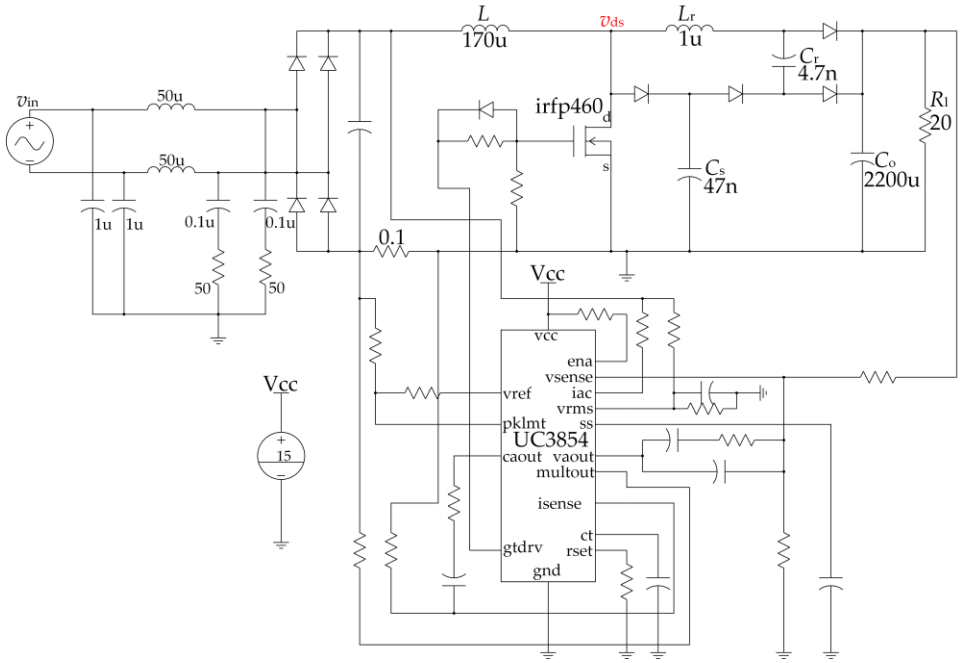

Figure 6. Boost PFC converter simulation circuit.

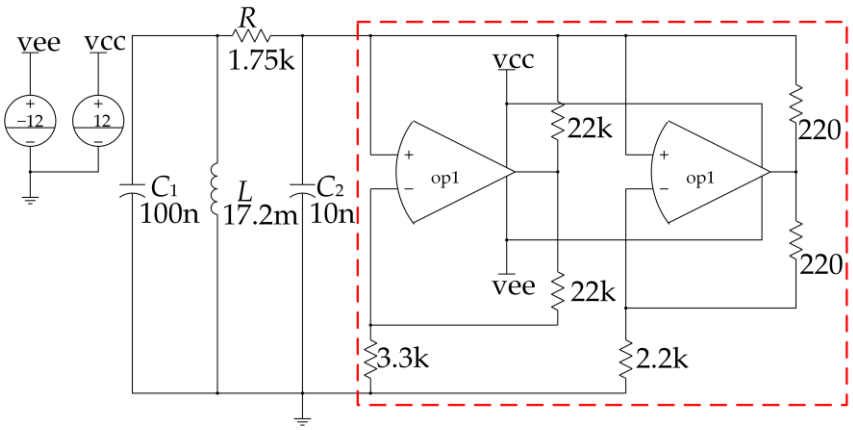

Figure 7. Chua's simulation circuit.

The simulation set up the probe to measure v_{ds}. The corresponding v_{ds} waveforms are shown in Figure 8a. According to Figure 8a, the lossless snubber reduces the rising rate of v_{ds} and reduces the du/dt of the switching. The spectrum of v_{ds} was obtained by fast

Fourier transform of the v_{ds} waveforms using Saber's waveform calculator. Moreover, the v_{ds} spectrum is shown in Figure 8b. According to the v_{ds} spectrum of the conventional circuit and lossless snubber in Figure 8b, we found that the peak of the v_{ds} spectrum of both the regular circuit and the lossless snubber (LS) occurs at the switching frequency and its multiples. Furthermore, in the high-frequency band, the peak spectrum of the lossless snubber is lower than that of the basic. This is consistent with the theoretical analysis.

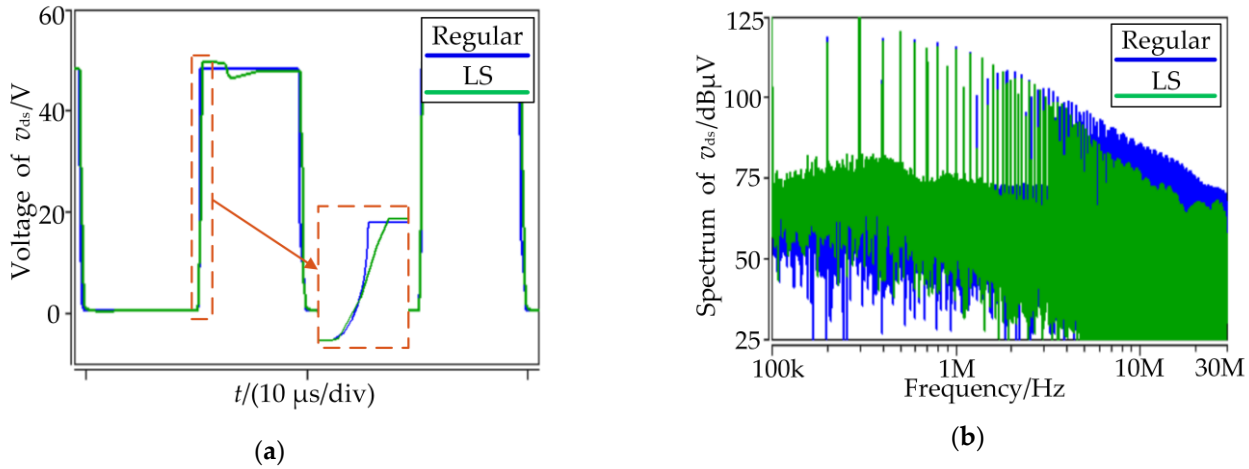

Figure 8. Drain–source voltage waveforms under regular and lossless snubbers: (**a**) Drain–source voltage waveform and (**b**) Drain–source voltage spectrum.

The lossless snubber PFC converter with traditional PWM (TPWM) and chaotic spread spectrum was simulated. Chaotic signals were generated using Chua's circuit with a spread spectrum of ±10 kHz. Furthermore, the spectrum of v_{ds} under TPWM and chaotic spread is shown in Figure 9. The simulation results show that the v_{ds} spectrum of CSS–LS has good continuity. The energy of the v_{ds} spectrum at the switching frequency and its multiples was dispersed to the surrounding frequencies by using CSS–LS. The energy dispersion reduces the peak value of the v_{ds} spectrum with CSS–LS. Compared to the v_{ds} spectrum with TPWM+LS, the peak of the v_{ds} spectrum with CSS–LS decreases significantly. At 300 kHz~10 MHz, the v_{ds} spectrum with CSS–LS is reduced by 6~20 dBμV compared to the v_{ds} spectrum of TPWM + LS. The simulation results verify the accuracy of the theoretical analysis, and the chaotic spread spectrum can optimize the EMI suppression effect of the lossless snubber.

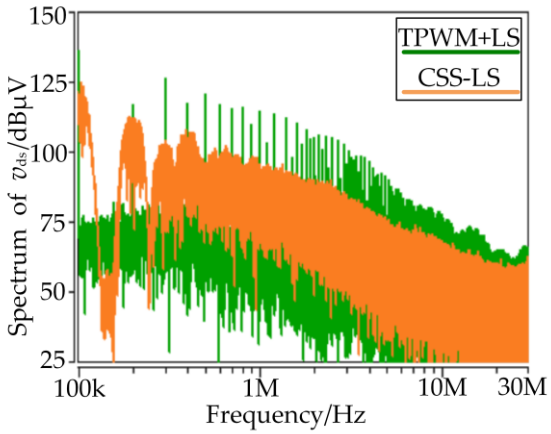

Figure 9. Drain–source voltage spectrum under TPWM and CSS–LS.

5. Results and Discussion

A prototype Boost PFC converter was built to verify the accuracy of the theoretical derivation and simulation. The experimental circuit diagram is shown in Figure 10. The prototype is shown in Figure 11. The inductor L of the prototype was measured to be 174 µH. The output capacitor C_o was selected to be 2200 µF. The load resistance R_l was selected to be 20 Ω. According to the Application note, the UC3854B was set up with a voltage feedback loop and a current feedback loop. Pin 12 of the UC3854B was connected to a resistor R_{set}, and pin 14 of the UC3854B was connected to a capacitor C_t. The values of R_{set} and C_t determined the oscillation frequency of the UC3854B. According to the Application note, the switching frequency of the prototype can be derived from the equation $f_s = 1.25/(R_{set} \times C_t)$. The switching frequency f_s of the prototype was calculated to be about 110 kHz. A programmable power supply provided the input power. The input voltage was 24 V, and the frequency was 50 Hz.

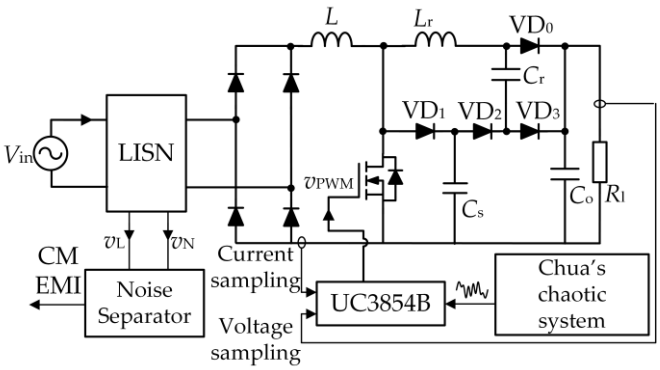

Figure 10. Circuit experiment.

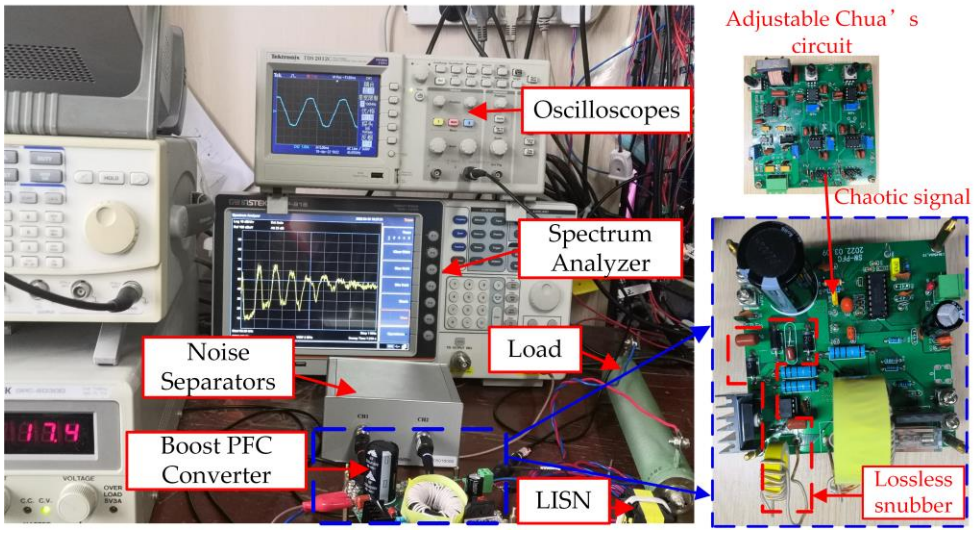

Figure 11. Experiment platform.

An adjustable Chua's circuit provided the chaotic signal. The attractor of the chaotic signal is shown in Figure 12a.The waveform of the sawtooth wave delayed by 1 s at Pin 14 of the UC3854 after spreading is shown in Figure 12b, with the switching signal jittering in the time domain.

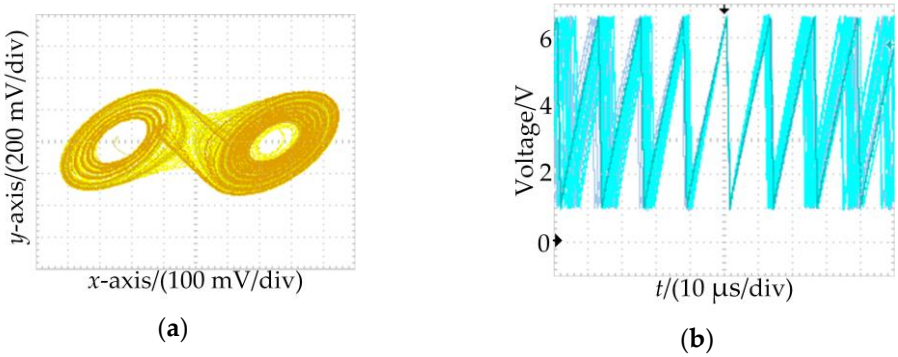

Figure 12. Chaotic spread spectrum: (**a**) Chaotic attractor and (**b**) Sawtooth waveform.

Firstly, an EMI test was carried out to measure the CM EMI spectrum of the PFC converter in the regular circuit, lossless snubber, and CSS–LS states. LISN was added between the input power supply and the prototype during the test. LISN represents the noise as a voltage. Then, the noise separator separated the CM EMI from the noise voltage. The spectrum of CM EMI was measured by the spectrum analyzer, as shown in Figure 13. The peak value of the CM EMI spectrum at switching frequency multipliers is shown in Table 2.

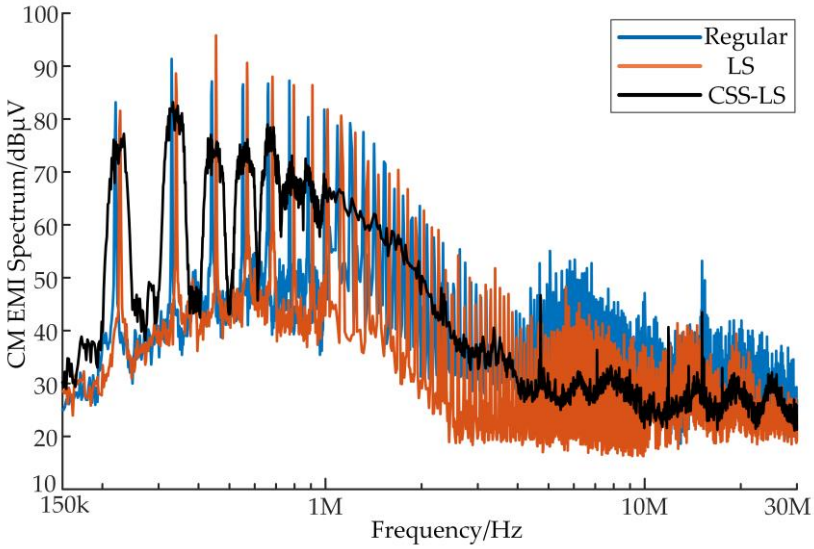

Figure 13. CM EMI spectrum.

Table 2. CM EMI spectrum at multiples of the switching frequency.

Frequency/Hz	**220 k**	**440 k**	**880 k**	**2.2 M**	**6.6 M**	**11 M**	**22 M**
Regular/dBµV	83.17	87.11	80.37	59.03	52.74	41.48	35.20
LS/dBµV	81.55	95.81	86.40	57.60	45.64	39.80	29.45
CSS–LS/dBµV	77.20	75.99	71.08	49.82	30.81	25.53	26.32

According to the spectrum of CM EMI, in 0.15~4 MHz, the spectrum of the lossless snubber is similar to that of the regular circuit. The CM EMI suppression effect of CSS–LS can be seen more clearly in Table 2 for the low-frequency band. In the low-frequency band, the CM EMI is not reduced or even higher for the circuit with a lossless snubber than the regular one. In comparison, the CM EMI with CSS–LS is reduced by 6~10 dBµV compared to the regular circuit. In 4~30 MHz, the peak of the CM EMI spectrum of lossless snubber is reduced by 4~10 dBµV. Comparing the CM EMI spectrum of basic circuits with that of CSS–LS, we found that the CM EMI spectrum of CSS–LS has good continuity. In

0.15~4 MHz, the peak CM EMI of CSS–LS is reduced by 6~20 dBμV compared to the basic. In 4~30 MHz, the CM EMI is reduced by 4~20 dBμV.

The experimental results show that CSS–LS significantly improves CM EMI suppression in low frequency compared to the lossless snubber circuits. The suppression effect in the high frequency is also better than that of the lossless snubber. It is consistent with the theoretical derivation and simulation analyses.

Finally, a power supply stability test was carried out. The input voltage, current, and output voltage of the PFC converter were measured under the regular circuit and CSS–LS state as shown in Figure 14. The CSS–LS has a negligible effect on the power factor correction, derived by comparing the input voltage and current sections in Figure 14. As in the conventional circuit, the phase of the input current in the CSS–LS state follows the input voltage very well. The power factor was 99.4% for the regular and 99.4% for CSS–LS. It shows that CSS–LS has less impact on the stability of the Boost PFC power supply.

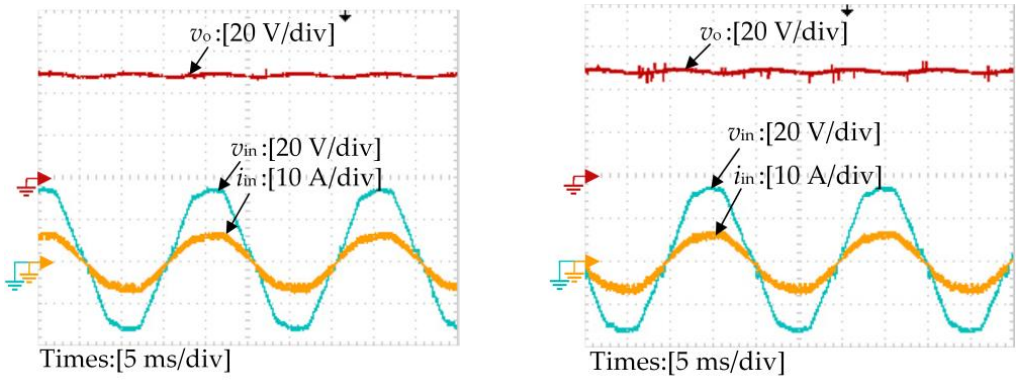

Figure 14. Input voltage and current and output voltage waveforms: (**a**) Regular Boost PFC converter and (**b**) Boost PFC converter with CSS–LS.

6. Conclusions

Aiming at the severe problem of EMI in high-frequency switching power supplies, this paper analyses the EMI suppression effect of lossless snubber by establishing a CM EMI model for lossless snubber PFC converters. A proposed CM EMI suppression method combines a passive lossless snubber circuit with a chaotic spread spectrum. This method improves the EMI suppression ability of the lossless snubber circuit at low frequencies. Moreover, it further reduces the peak of high-frequency EMI. At the same time, this method can reduce the switching loss and improve the converter's efficiency. Furthermore, it does not need to use an auxiliary circuit that is easy to apply. In addition, the CSS–LS only takes up a little space and is lightweight. Therefore, CSS–LS can be integrated into the converter circuit. Using CSS–LS to suppress CM EMI follows the trend of power electronic converters toward high-frequency and high-power density. CSS–LS can be used as an excellent CM EMI suppression method in high-power-density power electronic converters.

The final EMI test results show that CSS–LS reduces the CM EMI amplitude by 6~20 dBμV at a low frequency. The suppression effect in the high frequency is also better than that of the lossless snubber. The power supply stability tests also demonstrate that CSS–LS has little effect on the stability of the Boost PFC converter. Compared with other EMI suppression methods, this method requires fewer changes to the circuit structure and is less costly. The chaotic spread spectrum is suitable for PWM converters that use lossless buffers. This improved method not only reduces CM EMI but also reduces switching losses while taking up less space. This method, which is beneficial to high power density, has certain practical value.

Author Contributions: Conceptualization, W.F. and Y.C.; methodology, W.F.; software, Y.S.; validation, Y.S. and W.F.; investigation, W.F.; data curation, Y.S.; writing—original draft preparation, W.F.; writing—review and editing, Y.C.; project administration, Y.C. All authors have read and agreed to the published version of the manuscript.

Funding: This research received no external funding.

Data Availability Statement: Not applicable.

Conflicts of Interest: The authors declare no conflict of interest.

References

1. Wang, T.; Kao, Y.; Hung, S.; Wen, Y.; Yang, T.; Li, S.; Chen, K.; Zheng, K.; Lin, Y.; Lin, S.; et al. Monolithic GaN-Based Driver and GaN Switch With Diode-Emulated GaN Technique for 50-MHz Operation and Sub-0.2-ns Deadtime Control. *IEEE J. Solid-State Circuits* **2022**, *57*, 3877–3888. [CrossRef]
2. Wang, Y.; Ding, Y.; Yin, Y. Reliability of Wide Band Gap Power Electronic Semiconductor and Packaging: A Review. *Energies* **2022**, *15*, 6670. [CrossRef]
3. Tiwari, S.; Basu, S.; Undeland, T.M.; Midtgård, O. Efficiency and Conducted EMI Evaluation of a Single-Phase Power Factor Correction Boost Converter Using State-of-the-Art SiC Mosfet and SiC Diode. *IEEE Trans. Ind. Appl.* **2019**, *55*, 7745–7756. [CrossRef]
4. Lee, Y.; Yoo, J.; Hwang, I.; Sul, S. Analysis of Position Estimation Error in Signal-Injection Sensorless Control Induced by Inverter dv/dt-Based Current Measurement Noise. *IEEE Trans. Power Electron.* **2023**, *38*, 839–851. [CrossRef]
5. Gao, Z.; Zhang, J.; Huang, Y.; Guan, R.; Zhou, Y. A Closed-Loop Active Gate Driver of SiC MOSFET for Voltage Spike Suppression. *IEEE Open J. Power Electron.* **2022**, *3*, 723–730. [CrossRef]
6. Han, L.; Liang, L.; Kang, Y.; Qiu, Y. A Review of SiC IGBT: Models, Fabrications, Characteristics, and Applications. *IEEE Trans. Power Electron.* **2021**, *36*, 2080–2093. [CrossRef]
7. Nia, M.S.S.; Shamsi, P.; Ferdowsi, M. EMC improvement for high voltage pulse transformers by pareto-optimal design of a geometry structure based on parasitic analysis and EMI propagation. *CSEE J. Power Energy Syst.* **2021**, *7*, 1051–1063.
8. Xie, L.; Ruan, X.; Zhu, H.; Lo, Y. Common-Mode Voltage Cancellation for Reducing the Common-Mode Noise in DC–DC Converters. *IEEE Trans. Ind. Electron.* **2021**, *68*, 3887–3897. [CrossRef]
9. Yousef, A.M.; Ebeed, M.; Abo-Elyousr, F.K.; Elnozohy, A.; Mohamed, M.; Abdelwahab, S.M. Optimization of PID controller for hybrid renewable energy system using adaptive sine cosine algorithm. *Int. J. Renew. Energy Res.* **2020**, *10*, 670–677.
10. Yap, K.Y.; Beh, C.M.; Sarimuthu, C.R. Fuzzy logic controller-based synchronverter in grid-connected solar power system with adaptive damping factor. *Chin. J. Electr. Eng.* **2021**, *7*, 37–49. [CrossRef]
11. Elnozahy, A.; Yousef, A.M.; Ghoneim, S.S.; Abdelwahab, S.A.M.; Mohamed, M.; Abo-Elyousr, F.K. Optimal economic and environmental indices for hybrid PV/wind-based battery storage system. *J. Electr. Eng. Technol.* **2021**, *16*, 2847–2862. [CrossRef]
12. Liao, H.; Zhang, X.; Ma, H. Impedance-Shaping-Based Stability Control of Point-of-Load Converter Integrated with EMI Filter in DC Microgrids. *IEEE Access* **2022**, *10*, 25034–25043. [CrossRef]
13. Elnozahy, A.; Yousef, A.M.; Abo-Elyousr, F.K.; Mohamed, M.; Abdelwahab, S.A.M. Performance improvement of hybrid renewable energy sources connected to the grid using artificial neural network and sliding mode control. *J. Power Electron.* **2021**, *21*, 1166–1179. [CrossRef]
14. Hichem, L.; Amar, O.; Leila, M. Optimized ANN-fuzzy MPPT controller for a stand-alone PV system under fast-changing atmospheric conditions. *Bull. Electr. Eng. Inform.* **2023**, *12*, 1960–1981. [CrossRef]
15. Dai, H.; Torres, R.A.; Jahns, T.M.; Sarlioglu, B. Comparative Study of Conducted Common-Mode EMI in WBG-Enabled DC-Fed Three-Phase Current-Source Inverter. *IEEE J. Emerg. Sel. Top. Power Electron.* **2022**, *10*, 7188–7204. [CrossRef]
16. Natarajan, S.; Babu, T.S.; Balasubramanian, K.; Subramaniam, U.; Almakhles, D.J. A State-of-the-Art Review on Conducted Electromagnetic Interference in Non-Isolated DC to DC Converters. *IEEE Access* **2020**, *8*, 2564–2577. [CrossRef]
17. Zhang, Y.; Li, H.; Shi, Y. Electromagnetic Interference Filter Design for a 100 kW Silicon Carbide Photovoltaic Inverter Without Switching Harmonics Filter. *IEEE Trans. Ind. Electron.* **2022**, *69*, 6925–6934. [CrossRef]
18. Kumar, M.; Kalaiselvi, J. Analysis and Measurement of Non-Intrinsic Differential-Mode Noise in a SiC Inverter Fed Drive and Its Attenuation Using a Passive Sinusoidal Output EMI Filter. *IEEE Trans. Energy Convers.* **2023**, *38*, 428–438. [CrossRef]
19. Heller, M.J.; Krismer, F.; Kolar, J.W. EMI Filter Design for the Integrated Dual Three-Phase Active Bridge (D3AB) PFC Rectifier. *IEEE Trans. Power Electron.* **2022**, *37*, 14527–14546. [CrossRef]
20. Hoffmann, S.; Bock, M.; Hoene, E. A New Filter Concept for High Pulse-Frequency 3-Phase AFE Motor Drives. *Energies* **2021**, *14*, 2814. [CrossRef]
21. Han, Y.; Wu, Z.; Wu, D. Hybrid Common-mode EMI Filter Design for Electric Vehicle Traction Inverters. *Chin. J. Electr. Eng.* **2022**, *8*, 52–60. [CrossRef]
22. Zhang, Y.; Jiang, D. An Active EMI Filter in Grounding Circuit for DC Side CM EMI Suppression in Motor Drive System. *IEEE Trans. Power Electron.* **2021**, *37*, 2983–2992. [CrossRef]

23. Zhou, Y.; Chen, W.; Yang, X.; Zhang, R.; Yan, R.; Liu, J.; Wang, H. A New Integrated Active EMI Filter Topology with Both CM Noise and DM Noise Attenuation. *IEEE Trans. Power Electron.* **2022**, *37*, 5466–5478. [CrossRef]
24. Li, H.G.; Gong, S.D.; Liu, J.W.; Su, D.L. CMOS-Based Chaotic PWM Generator for EMI Reduction. *IEEE Trans. Electromagn. Compat.* **2017**, *59*, 1224–1231. [CrossRef]
25. Li, H.; Ding, Y.; Zhang, C.; Yang, Z.; Yang, Z.; Zhang, B. A Compact EMI Filter Design by Reducing the Common-Mode Inductance with Chaotic PWM Technique. *IEEE Trans. Power Electron.* **2022**, *37*, 473–484. [CrossRef]
26. Ji, Q.; Ruan, X.; Ye, Z. The Worst Conducted EMI Spectrum of Critical Conduction Mode Boost PFC Converter. *IEEE Trans. Power Electron.* **2015**, *30*, 1230–1241. [CrossRef]
27. Mohammadi, M.R.; Peyman, H.; Yazdani, M.R.; Mirtalaei, S.M.M. A ZVT Bidirectional Converter with Coupled-Filter-Inductor and Elimination of Input Current Notches. *IEEE Trans. Ind. Electron.* **2020**, *67*, 7461–7469. [CrossRef]
28. Mohammadi, M.; Adib, E.; Yazdani, M.R. Family of Soft-Switching Single-Switch PWM Converters with Lossless Passive Snubber. *IEEE Trans. Ind. Electron.* **2015**, *62*, 3473–3481. [CrossRef]
29. Lee, S.; Do, H. A Single-Switch AC–DC LED Driver Based on a Boost-Flyback PFC Converter with Lossless Snubber. *IEEE Trans. Power Electron.* **2017**, *32*, 1375–1384. [CrossRef]
30. Yano, Y.; Kawata, N.; Iokibe, K.; Toyota, Y. A Method for Optimally Designing Snubber Circuits for Buck Converter Circuits to Damp LC Resonance. *IEEE Trans. Electromagn. Compat.* **2019**, *61*, 1217–1225. [CrossRef]
31. Yau, Y.; Hung, T. Lossless Snubber for GaN-Based Flyback Converter with Common Mode Noise Consideration. *IEEE Access* **2022**, *10*, 56652–56667. [CrossRef]
32. Wu, Y.; Yin, S.; Li, H.; Ma, W. Impact of *RC* Snubber on Switching Oscillation Damping of SiC MOSFET with Analytical Model. *IEEE J. Emerg. Sel. Top. Power Electron.* **2020**, *8*, 163–178. [CrossRef]
33. Han, W.; Cheng, Q.; Chen, C.; Lee, H. Conductive EMI Reduction Techniques for Soft-switched Half-bridge Buck Converters in Automotive Applications. In Proceedings of the 2022 IEEE Applied Power Electronics Conference and Exposition (APEC), Houston, TX, USA, 20–24 March 2022.
34. Yang, R.; Zhang, B. Experiment and mechanism research of chaotic PWM of converter in EMI suppressing. *Proc. CSEE* **2007**, *10*, 114–119.
35. Yu, X.; Su, J.; Guo, S.; Zhong, S.; Shi, Y.; Lai, J. Properties and Synthesis of Lossless Snubbers and Passive Soft-Switching PWM Converters. *IEEE Trans. Power Electron.* **2020**, *35*, 3807–3827. [CrossRef]